Journal of Hydrology 522 (2015) 382–390

Contents lists available at ScienceDirect

Journal of Hydrology

journal homepage: www.elsevier.com/locate/jhydrol

The contribution of atmospheric rivers to precipitation in Europe and the United States

David A. Lavers *, Gabriele Villarini

IIHR-Hydroscience & Engineering, The University of Iowa, Iowa City, IA, USA

ARTICLE INFO

Article history:
Received 10 January 2014
Received in revised form 2 December 2014
Accepted 8 December 2014
Available online 16 December 2014
This manuscript was handled by Andras Bardossy, Editor-in-Chief, with the assistance of Uwe Haberlandt, Associate Editor

Keywords:
Atmospheric rivers
Water budget
Precipitation
Zero-inflated beta regression
Europe
Continental United States

SUMMARY

Atmospheric rivers (ARs) are narrow corridors within the warm conveyor belt of extratropical cyclones in which the majority of the poleward water vapour transport occurs. These filamentary synoptic features are responsible for extreme precipitation and flooding in Europe and the central and western United States, and also play an essential role for water resources in these areas. Using gridded precipitation products across Europe and the continental United States and the ERA-Interim reanalysis, we investigate the fraction of precipitation from 1979 to 2012 that is related to ARs in these regions. The results are region- and month-dependent, with the largest contribution generally occurring during the winter season and being on the order of 30–50%. This is particularly true for Western Europe, the U.S. West Coast, and the central and northeastern United States. Our results suggest that ARs are important agents for water supply in Europe and the United States. We have also examined whether there have been changes over time in the fractional contribution of ARs to seasonal rainfall using zero-inflated beta regression. We find that there has been a decrease in the average AR-contribution over the Mediterranean region and over the central United States.

1. Introduction

Extratropical cyclones are an important mechanism of precipitation in the extratropics (Stewart et al., 1998), and have been shown to play a key role in mid-latitude extreme precipitation events (e.g., Pfahl and Wernli, 2012). A recent study by Hawcroft et al. (2012) investigated the proportion of precipitation associated with extratropical cyclones using reanalysis and satellite-based precipitation products. In particular, they showed that in parts of Europe and North America more than 70% of total precipitation could be attributed to extratropical cyclones. Another study by Catto et al. (2012) investigated the amount of precipitation related to fronts, features which form an integral part of extratropical storms, and concluded that up to 90% of precipitation was associated with fronts in the main storm track regions of the Northern Hemisphere (North Pacific and North Atlantic). These results highlight the important role that extratropical cyclones play in the mid-latitude water budget.

The poleward transport of sensible and latent heat occurs in the extratropical cyclone's warm conveyor belt (WCB). At low altitudes (< ~2.5 km) in the pre-cold-frontal region within the WCB a combination of high moisture content and the low-level jet (LLJ) results in a narrow region responsible for the vast majority of the water vapour (or latent heat) transport; this region is called an *atmospheric river* (AR). The AR region has been known for some time (Browning and Pardoe, 1973), and research has found strong relationships between ARs and heavy rainfall and flooding in the mid-latitudes, in particular over western North America (e.g., Ralph et al., 2006; Neiman et al. 2011; Ralph and Dettinger, 2012), the central United States (Moore et al., 2012; Nakamura et al., 2013; Lavers and Villarini, 2013a), South America (e.g., Viale and Nunez, 2011), the British Isles (Lavers et al., 2011, 2012), and continental Europe (Lavers and Villarini, 2013b). For example, in the Russian River basin in northern California Ralph et al. (2006) found that the seven recorded floods (from 1998 to 2006) were caused by ARs; in Europe Lavers and Villarini (2013b) showed that areas, such as Scotland and the Iberian Peninsula, had 7 of the top 10 daily annual maxima precipitation events related to ARs.

In the western United States research has considered the role ARs have in precipitation occurrence, as opposed to considering the precipitation from the whole of extratropical cyclones, as in Hawcroft et al. (2012). Dettinger et al. (2011) estimated that over

* Corresponding author at: Center for Western Weather and Water Extremes, Scripps Institution of Oceanography, University of California San Diego, La Jolla, California. Tel.: +1 858 534 3320.
E-mail address: dlavers@ucsd.edu (D.A. Lavers).

http://dx.doi.org/10.1016/j.jhydrol.2014.12.010
0022-1694/

1998–2008 ARs were responsible for 20–50% of California's precipitation and streamflow. Furthermore, this precipitation was delivered in a few AR storms, highlighting the importance of ARs for water supplies in California. Rutz and Steenburgh (2012) investigated the AR contribution to precipitation across the western United States (over 1998–2008) using ARs identified as far south as 24°N (to include Baja Peninsula), and by including high-elevation snowpack telemetry sites. They found good agreement with the results of Dettinger et al. (2011), and found that including ARs crossing the Baja Peninsula led to increased AR fraction over the southwestern United States. More recently, Rutz et al. (2014) expanded on these previous two studies providing information about the climatological characteristics of ARs and their inland penetration.

A literature review uncovered no studies that have attempted to characterize the contribution of ARs to precipitation over Europe or the eastern half of the United States. Moreover, the research related to AR contributions to the water budget has focused only on limited time periods (i.e., a decade or so). To address these research gaps, we focus on the period 1979–2012 (34 years) with the goal of evaluating the importance of ARs to precipitation over Europe and the continental United States. Finally, despite the importance of ARs as a source of terrestrial moisture, we currently do not know whether there has been a change (either positive or negative) in the fractional contribution of ARs to seasonal precipitation over Europe or the continental United States. Here we will provide insight on this issue by developing zero-inflated beta regression models.

2. Data and methods

The specific humidity, and the zonal and meridional wind fields were retrieved from the European Centre for Medium-Range Weather Forecasts (ECMWF) ERA-Interim (ERAIN) reanalysis at a $0.7° \times 0.7°$ resolution over 1979–2012 (Dee et al., 2011). The vertically-integrated horizontal water vapour transport (hereafter, integrated vapour transport, IVT) was calculated from 1000 hPa to 300 hPa in an Eulerian framework (e.g. Neiman et al., 2008). The IVT fields were used in AR detection algorithms developed for Europe in Lavers and Villarini (2013b), and for the central United States in Lavers and Villarini (2013a). We applied a modified version of the European algorithm for the western United States. A brief description of the algorithm in the three regions is given below.

Initially we computed IVT thresholds that are used to identify AR occurrence. For Europe (between 30°N and 70°N near 10°W) and the western United States (between 25°N and 50°N along the coast) a latitude-dependent IVT threshold was calculated as follows. At 1200 UTC on each day from 1979 to 2012 we extracted the maximum IVT (between 30°N and 70°N near 10°W; between 25°N and 50°N along the U.S. West Coast) and binned it into 5-degree latitude bins. The median of the IVT in each latitude bin was used as the threshold value for ARs identified in that region. The IVT thresholds in each band in Europe are given in Supplementary Table 1; for the western United States the IVT thresholds are given in Supplementary Table 2. For the central and eastern United States a threshold was determined by extracting the maximum IVT at 1200 UTC on each day from 1979 to 2012 between 110°W and 70°W near 40°N, and then calculating the median value; the IVT threshold was 367.8 kg m^{-1} s^{-1}.

To identify ARs striking the western European boundary between 30°N and 70°N at 10°W, we applied a modified version of the algorithm described in Lavers and Villarini (2013b) at each ERAIN six hour time step from 1979 to 2012. We calculated the IVT at grid points spanning between 30°N and 70°N along 10°W and retained the maximum IVT value and location. If the maximum IVT value exceeded the IVT threshold for that particular latitudinal bin, the grid point was recorded. We then searched for the maximum IVT along each meridian from 10°W to 30°W, and tracked the location of the grid points where the IVT threshold (taken from 10°W) was exceeded. We also searched for the maximum IVT along each meridian from 10°W to 25°E recording the locations where the IVT threshold was exceeded. Finally, we determined whether the extracted points satisfied the criterion of an appropriate length scale. If 30 continuous longitude points (with no more than a 3° latitude displacement between each set of points) exceeded the threshold (on average across the domain this is roughly equal to 1500 km), we considered it an AR time step. We also ran the above AR algorithm at 5°E (using the same IVT thresholds from 10°W) to identify ARs that would not be detected at 10°W (thus more closely capturing AR penetration into Europe). The only difference in the algorithm was that the maximum IVT between 30°N and 70°N along 5°E was identified, and then we searched for the maximum IVT along each meridian from 5°E to 15°W and 5°E to 25°E.

To identify ARs striking the western United States between 25°N and 50°N, the following methodology was used at each ERAIN six hour time step from 1979 to 2012. We calculated the IVT at grid points spanning between 25°N and 50°N (along the coast) and retained its maximum value and location. If the maximum value exceeded the threshold for that particular region, the grid point was recorded. We then searched for the maximum IVT along each meridian up to 20° westwards from the coast, and tracked the location for the grid points where the IVT threshold (taken from the coast) was exceeded. We also searched for the maximum value along each meridian from the coast to 100°W recording the locations where the threshold was exceeded. Finally, we determined whether the extracted points satisfied the criterion of an appropriate length scale. If 30 continuous longitude points (with no more than a 3° latitude displacement between each set of points) exceeded the threshold, we considered it as an AR time step.

For the central and eastern United States the following methodology was used at each six hour time step in the ERAIN reanalysis over the study period; this is a slightly modified version of the algorithm presented in Lavers and Villarini (2013a). We calculated the IVT at grid points spanning 66°W and 110°W along 40.35°N and retained its maximum value. If the IVT at 40.35°N exceeded the threshold, we searched for the maximum value along each parallel from 40°N to 25°N, and tracked the location for the grid points where the IVT threshold was exceeded. We also searched for the maximum IVT along each parallel from 40°N to 50°N, and tracked the location for the grid points where the threshold was exceeded. If 13 continuous longitude points (with no more than a 3° longitude displacement between each set of points) exceeded the threshold, we considered it as an AR time step. Furthermore, any days when a North Atlantic tropical cyclone was present between 25°N and 50°N, and 110°W and 70°W were excluded from the analysis.

For Europe we retrieved daily observed gauge-based precipitation produced by the ENSEMBLES project (Haylock et al., 2008) at a $0.25° \times 0.25°$resolution (E-OBS version 7.0 data set). Data from 1979 to 2012 were used and these represent daily accumulations from 00UTC to 00UTC. Over the United States we used the Climate Prediction Center (CPC) Unified Gauge-Based Analysis of Daily Precipitation (http://www.esrl.noaa.gov/psd/data/gridded/data.unified.daily.conus.html) as the reference dataset. Data from 1979 to 2012 were used and represent daily accumulations at 12UTC at a $0.25° \times 0.25°$ resolution. This dataset is based on precipitation measurements from the National Oceanic and Atmospheric Administration (NOAA)'s National Climate Data Center (NCDC) daily COOP stations, daily accumulations from hourly precipitation

datasets, and data from River Forecast Centers and 1st order stations (Higgins et al., 2000).

To associate precipitation at a grid point with an AR, the precipitation pixel had to have a Euclidian distance of less than 1.5° from a point on the axis of an AR (as detected by the AR algorithm). As the AR axis is considered to be the center of the AR, a 1.5° distance only includes precipitation in the vicinity of the AR in an approximate 300 km swath around the AR center (and not in the broader WCB region of extratropical cyclones). Note that even if only one six-hour time step in a day has an AR detected, we consider that the precipitation accumulation on that day (at a grid less than 1.5° from the AR axis) is AR-related.

3. Zero-inflated beta regression

Modeling of the temporal changes in the fraction of AR contribution to rainfall over Europe and the continental United States is performed by means of beta regression, which is used to describe rates and proportions (e.g., Ferrari and Cribari-Neto, 2004). In a beta regression model, the predictand can assume values between 0 and 1 (extremes excluded). The beta distribution does not belong to the exponential family, like the binomial, Gaussian or Poisson distributions, and therefore it is outside of the distributions that can be fitted with a generalized linear model (e.g., McCullagh and Nelder, 1989; Dobson, 2001). Instead, we use the Generalized Linear Model in Location, Scale and Shape (GAMLSS; Rigby and Stasinopoulos, 2005; Stasinopoulos and Rigby, 2007), which provides a high degree of flexibility in the selection of the distribution. The probability density function (pdf) of the beta distribution can be written as:

$$p(y_i|\theta,\eta) = \frac{1}{B(\theta,\eta)} y_i^{\theta-1}(1-y_i)^{\eta-1} \tag{1}$$

where $y_i \in (0,1)$ is the AR-fraction for the ith year, $B(\cdot)$ is the beta function, $\theta > 0$ and $\eta > 0$. We use the GAMLSS reparameterization (Ferrari and Cribari-Neto, 2004; Stasinopoulos et al., 2009), in which $\mu = \left(\frac{\theta}{\theta+\eta}\right)$ and $\sigma = \left(\frac{\theta}{\theta+\eta+1}\right)$ when $\mu \in (0,1)$ and $\sigma \in (0,1)$. The first and second moments of y are μ and $\sigma^2\mu(1-\mu)$, respectively.

The classic two-parameter beta distribution does not include 0 and 1 in the support of the predictand. Our time series, however, can have zero values. The issue related to the presence of zeros can be addressed by using the three-parameter zero-inflated beta distribution (Ospina and Ferrari 2010), in which the additional parameter allows y to be equal to zero (it models the probability at zero). The pdf of the zero-inflated beta distribution can be written as:

$$\begin{cases} p(y_i) = \nu & \text{if } y_i = 0 \\ p(y_i|\mu,\sigma) = (1-\nu)\frac{\Gamma(\sigma)}{\Gamma(\mu\sigma)\Gamma((1-\mu)\sigma)} y_i^{\mu\sigma}(1-y_i)^{((1-\mu)\sigma)-1} & \text{if } y_i \in (0,1) \end{cases} \tag{2}$$

where the parameters $\mu \in (0,1)$, σ is strictly positive and $\nu \in (0,1)$. The expected value of y is equal to $(1-\nu)\cdot\mu$ and the variance is equal to $(1-\nu)\left(\frac{\mu(1-\mu)}{\sigma+1}\right) + \nu(1-\nu)\mu^2$. We use a logit link function for μ and ν, and a logarithmic link function for σ to satisfy the conditions on the parameters. The zero-inflated beta distribution is very flexible. It can be symmetric or highly asymmetric depending on the values of the parameters, with a mass of probability at zero (Supplementary Fig. 1; see also Ospina and Ferrari (2010)). An even more general modeling would be by considering a zero-one inflated beta distribution, allowing the modeling of the probability of 0 and 1. Because of the lack of 1 in our datasets, we focus on the zero-inflated beta distribution.

We examine changes over time t (from 1979 to 2012) in the three parameters of the zero-inflated beta distribution using the following simple dependences:

$$\begin{cases} \mu = exp\left(\frac{\alpha_0+\alpha_1 t}{1-\alpha_0-\alpha_1 t}\right) \\ \sigma = exp(\beta_0+\beta_1 t) \\ \nu = exp\left(\frac{\gamma_0+\gamma_1 t}{1-\gamma_0-\gamma_1 t}\right) \end{cases} \tag{3}$$

We consider all the possible model combinations in which each of the three parameters is allowed to be a linear function of time as in Eq. 3 or constant. To avoid model overfit, model selection is performed with respect to the Akaike Information Criterion (AIC; Akaike, 1974) which represents a trade-off between the complexity and the accuracy of the models. Because of numerical issues associated with the convergence of the algorithm to estimate the models' parameters, we fit these models only over pixels with less than 26 (out of 34) zeros.

All the calculations are performed in R (R Development Core Team, 2012) using the freely available gamlss package (Stasinopoulos et al., 2007).

4. Results and discussion

The two left panels of Fig. 1 show the average monthly precipitation (over the period 1979–2012) in Europe and the continental United States. The western coasts (e.g. Pacific Northwest and Norway) receive the highest precipitation totals with values in excess of 250 mm/month due to their location in the extratropical storm track, and owing to the hills/mountains that cause orographic enhancement of precipitation. An arc of precipitation totals exceeding about 150 mm is also found along the European Alps. The dry interior western United States are clearly seen by precipitation values of less than 25 mm/month, while a large region along the U.S. Gulf Coast has average monthly precipitation between 100 mm and 150 mm. The average monthly AR fraction is shown in the right panels of Fig. 1. In Europe, the highest percentages (~20–30%) are found from the western Iberian Peninsula to western France. The AR fraction reduces as the distance inland increases in part because ARs weaken as they propagate inland. There is little AR impact in southern Europe (eastern Spain, southern France, and Italy), which is probably a result of the mountains in Spain which block ARs from penetrating there. In the western United States there is less AR penetration into the interior than in Europe due to the larger mountains close to the coast (e.g., Cascade Range from Washington through Oregon to northern California); the highest AR fraction percentages peak at about 25% in northern Oregon. In the eastern United States, New England has the highest AR fraction of greater than 30%, while the central United States has values of above 25% along the Mississippi valley (centered on western Tennessee), and a smaller area of AR fraction greater than 20% over northern Missouri/southern Iowa. Previous research for the central United States has shown strong connections between ARs and flooding (Lavers and Villarini, 2013a; Nakamura et al., 2013), and between an AR event and extreme precipitation in Tennessee in May 2012 (Moore et al., 2012), which underscores the importance of ARs in this part of the United States. The Appalachian Mountains are clearly visible as a low AR fraction region dividing relatively high percentages along the U.S. East Coast and the central United States.

While Fig. 1 provides results related to the AR contribution to rainfall at the yearly scale, Figs. 2 and 3 provide more detailed information about the AR contribution on a monthly scale. As shown in Fig. 2 for Europe, it is evident that the largest and most widespread values occur during the winter half-year (October to

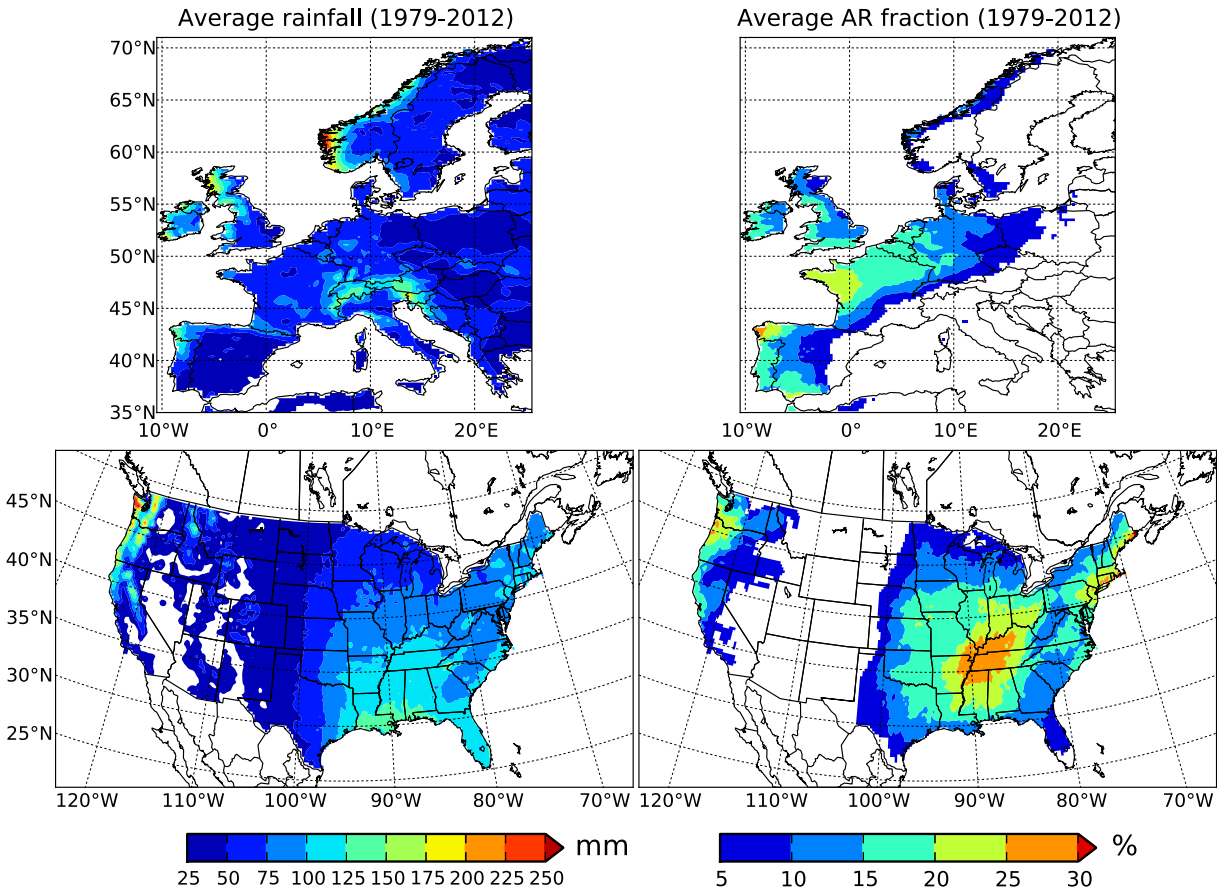

Fig. 1. The average monthly precipitation (in mm) (left panels), and average monthly AR fraction (in%; right panels) in Europe (top panels) and the United States (bottom panels) over 1979 to 2012.

March), not only along the coast but as far inland as Poland and Lithuania. During the winter, the North Atlantic storm track is more active due to the stronger Equator-North Pole temperature gradient (resulting in a stronger baroclinic zone), and hence extratropical cyclones (in which ARs occur) are more prevalent. Maximum AR fraction values of greater than 30% are found from October to January in France and Spain (and Belgium and the Netherlands in January). Visual inspection of the average precipitation in January (Supplementary Fig. 2) implies that in northern France about 25 mm of the average 75 mm is caused by ARs; in north-western Spain it is approximately 60 mm of the climatological average of about 180 mm. Note that these values are obtained over a 34-year period, with values in certain years being much larger than the average percentages (which in certain cases can be related to intense single ARs). A clear west-southwest to east-northeast oriented line exists across southern Europe (from the France/Spain border to central Europe) bounding low AR faction to the south and relatively high AR fraction to the north. In Norway there are lower AR fraction values than potentially expected, especially considering the mountainous terrain there. It is furthermore unexpected because a strong link has been shown in Norway between annual maxima daily precipitation and ARs in previous research (Fig. 3; Lavers and Villarini, 2013b). The summer months have the lowest AR fraction values because a weaker equator-to-North Pole temperature gradient and North Atlantic storm track means that fewer extratropical cyclones occur, and thus the AR effect on precipitation is weaker. In summer precipitation tends to be more related to smaller scale convective weather systems (e.g. Berg et al., 2009). Also, the high AR fraction in southern Portugal in June and July (Fig. 2) is probably not particularly important because the fraction is of such a small climatological precipitation (Supplementary Fig. 2).

In the western United States the largest and most widespread AR fraction values are seen from October to February (Fig. 3). For example in November in Oregon there are AR fraction values of up to 35%, which when considering the climatological precipitation (greater than 250 mm; Supplementary Fig. 3) amounts to about 100 mm of the precipitation. As in Europe there are smaller AR fractions found in the summer, which is again due to a weaker summer storm track across the North Pacific. In general the AR fractions in this study are lower than those presented in Rutz and Steenburgh (2012), Dettinger et al. (2011), and Rutz et al. (2014). Possible reasons for the discrepancies are: (1) the different methodologies employed to identify ARs. Herein a strict distance criterion (of 1.5°) for precipitation to be AR related is used, whereas for example Rutz and Steenburgh (2012) consider that if an AR occurs anywhere on the West Coast all western U.S. precipitation is said to be AR related [a more regional approach was employed by Rutz et al. (2014) even though it is likely that they would identify a larger AR contribution than in this study (see their Fig. 3)]; (2) we undertake monthly AR fraction analyses, whereas a November–April seasonal analysis was assessed in Rutz and Steenburgh (2012), and Dettinger et al. (2011); and (3) the past studies only used the water years 1998–2008 compared to the 1979–2012 period used herein (1988–2011 in Rutz et al. (2014)).

In the eastern and central United States the AR fraction is the highest in November and December, with a region focussed on Tennessee and Kentucky having maximum percentages larger than 45%. In December this means that about 60 mm of the climatological precipitation of about 125 mm is AR related (see Fig. 3 and

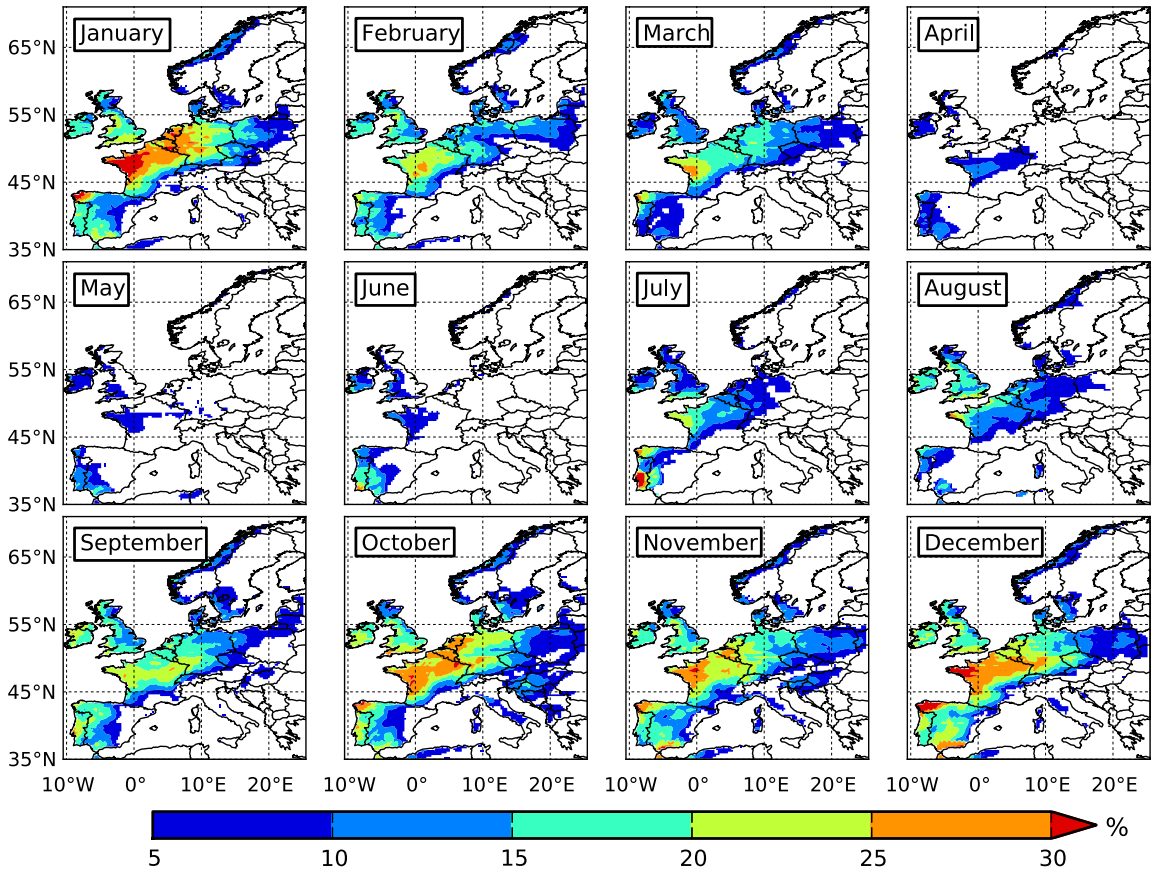

Fig. 2. The average AR fraction (in%) in each month from Europe over the period 1979–2012.

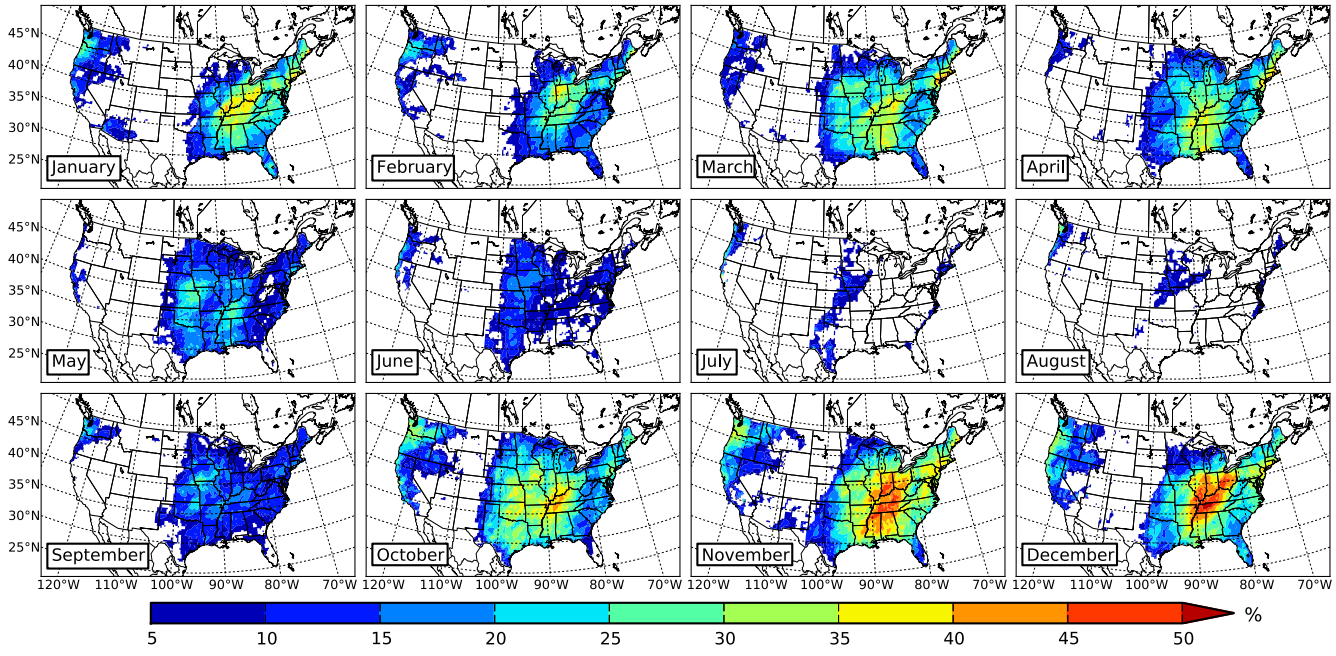

Fig. 3. Same as Fig. 2 but for the continental United States.

Supplementary Fig. 3). This region is affected by extratropical cyclones that travel eastwards across the United States, and the circulation advects moisture northward in the warm sector of the storm from the Gulf of Mexico. In spring and early summer (e.g. May and June) an area of significant AR fraction extends from Texas to the Great Lakes (to the west of the highest AR fraction region in winter). The high moisture transport found in some ARs at this time of the year is in part due to the Great Plains LLJ, and such

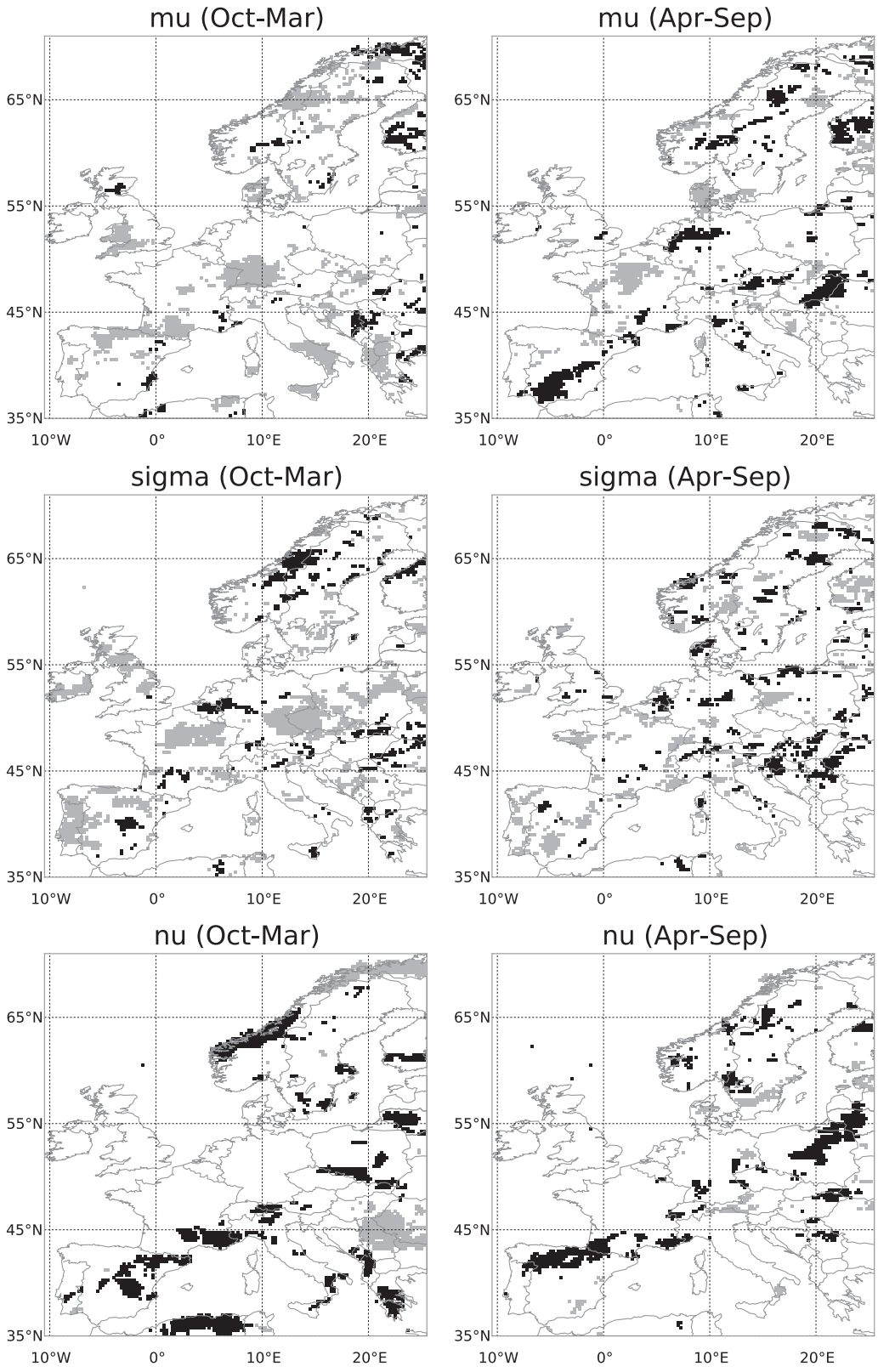

Fig. 4. Maps showing the results for the zero-inflated beta regression for Europe for the parameter μ (top panels), σ (middle panels), and ν (bottom panels) for the cold (left panels) and warm (right panels) seasons. The black (grey) colors indicate an increase (a decrease) over time. The white areas are for pixels in which there is no temporal dependence over time.

ARs were behind the U.S. Midwest flooding of July 1993 and June 2008 (Dirmeyer and Kinter, 2009; Lavers and Villarini, 2013a). It is noticeable how the Appalachian Mountains act as a boundary between areas of relatively high AR fraction in the central and eastern United States. This is especially clear in the top and bottom rows of Fig. 3. In the north-eastern United States the high AR

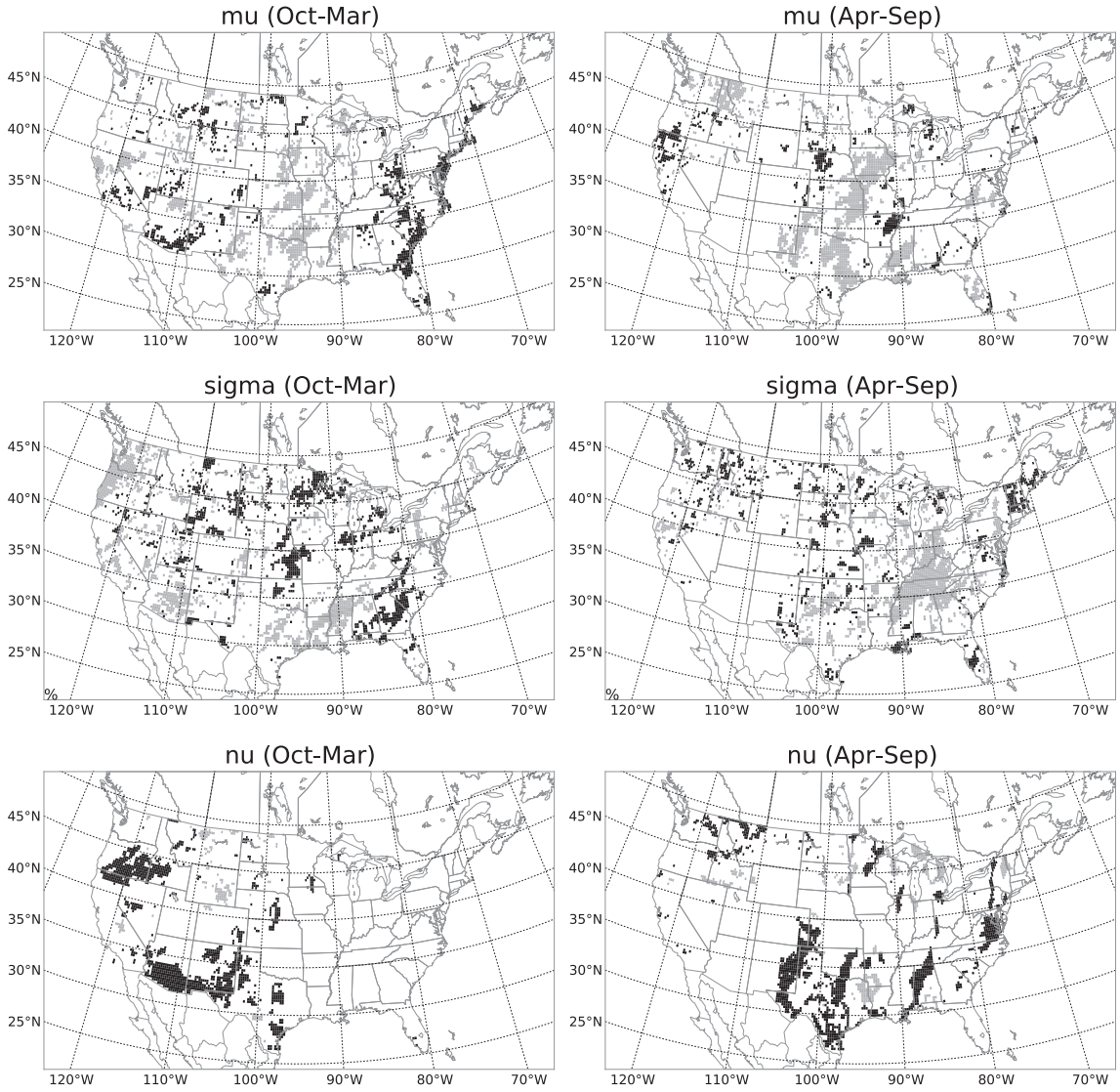

Fig. 5. Same as Fig. 4 but for the continental United States.

fraction percentages in winter are thought to be indicative of snowfall events, such as the heavy snow events in the winter of 2009 to 2010 (Halverson and Rabenhorst, 2010).

The results so far point to the significant role played by ARs in bringing atmospheric moisture vital for water resources in large areas of Europe and the continental United States. Little is known about how the AR contribution to precipitation has been changing over the past three decades. To address this question, we use the zero-inflated beta regression model described in Section 3 to examine possible changes in the fractional contribution of ARs to precipitation over Europe and the continental United States. Because of the marked seasonality and for conciseness, we perform the analyses by stratifying the data into two seasons, cold (from October to March) and warm (from April to September). Moreover we focus our discussion on the μ and ν parameters because they are directly related to the probability of zeros and to the mean (σ is related to the variance, but not by itself but as a non-linear combination of all the three parameters). Fig. 4 summarizes the results for Europe. During the cold season (Fig. 4, left panels) the most regionally consistent pattern of change is in the Mediterranean region, in which we observe an increase over time in the parameter ν, which translates to an increase in the probability of zero-AR contribution to the seasonal rainfall over the area. We also observe a decrease over time in the parameter μ indicating a decrease in the average AR contribution to the seasonal rainfall over the period 1979–2012; this possibly relates to a drying of the Mediterranean region (e.g., Klein Tank and Können, 2003; van den Besselaar et al., 2013) and a poleward shift in the North Atlantic extratropical cyclone tracks (e.g., Yin, 2005; Zappa et al., 2013). The results for the warm season (Fig. 4, right panels) are generally similar to those discussed for the cold season.

Fig. 5 summarizes the results for the continental United States. The largest regional changes in the ν parameters are over the southwest United States and Oregon during the cold season and over Texas and Oklahoma during the warm season. In both cases, the results point to an increase over time in the probability of zero-AR contribution to the seasonal precipitation. The largest changes in the μ parameter for both the cold and warm seasons are over the central United States from Texas to Iowa. More specifically, we observe a decrease over time in this parameter, leading to a decrease in the average AR contribution to precipitation over this region. These results are consistent with Barandiaran et al. (2013) who found a northward expansion of the Great Plains LLJ over the same study period during the April–June months.

Moreover, they found a decrease in total precipitation south of 40°N, which is similar to the areas that have been experiencing an average reduction in AR-related precipitation. These results are also in line with the modeling work by Cook et al. (2008) which showed a strengthening in the Great Plains LLJ in response to an increase in greenhouse gasses, leading to an increase in precipitation in the Upper Mississippi region and a decrease in the southern Great Plains.

5. Conclusions

The aim of this paper was to evaluate the contribution of ARs to the water budget in Europe and the continental United States by computing the percentage of precipitation that was related to ARs over the period 1979–2012. We draw the following conclusions from this study:

- Over the study period, we show that ARs are responsible for about 20–30% of all precipitation in parts of Western Europe, and the central and western United States. Western Europe and the western United States have relatively large AR fractions because hills and mountains cause orographic enhancement of precipitation when an AR impacts the higher terrain.
- The effects of ARs are generally felt further inland in Europe (e.g. Poland) than in the western United States, which is likely to be due to the higher mountainous terrain in the latter which acts as a barrier to inland penetration. However, AR impacts can be significant in the interior of the western United States, as shown for Arizona by Neiman et al. (2013).
- Strong seasonality exists in the largest AR fractions and in their spatial extent ranging from a peak in the fall and winter to a minimum in the summer. In Europe, AR fractions peak at about 30% in the fall and winter (mainly in France and Spain); in the western United States we find a similar seasonality, with AR fractions up to about 35% in Oregon; the central United States has generally even larger values during the cold season, with some regions having values in excess of 50% (e.g., Tennessee in December). It is during the winter half-year that the storm tracks in the North Atlantic and Pacific (in which extratropical cyclones grow and propagate along) are more active resulting in more AR activity, and thus higher AR fractions. Note that although relatively low AR fractions occur in the central United States in the summer, this is the time when ARs can cause the most extreme flood events (as during the summer of 1993 and June 2008).
- We have examined potential changes in the fractional contribution of ARs to seasonal precipitation using a zero-inflated beta regression model. Over the past three decades, our results point to a reduced contribution of ARs to regional precipitation in particular over the Mediterranean region and the central United States. These findings are consistent with a poleward shift in the North Atlantic storm track and the Great Plains LLJ. These results should not be viewed necessarily as a reduction in precipitation over these areas, but just in light of the role played by ARs.
- It is also thought that this type of analysis may be used as a model diagnostic to determine how well numerical weather prediction models can capture the water budget (associated with ARs) compared to reanalysis datatsets (such as ERAIN).

Acknowledgments

The authors gratefully acknowledge financial support by IIHR-Hydroscience & Engineering and the Iowa Flood Center. Gabriele Villarini also acknowledges financial support from the USACE Institute for Water Resources. We used the E-OBS dataset from the EU-FP6 project ENSEMBLES (http://ensembles-eu.metoffice.com) and thank data providers in the ECA&D project (http://eca.knmi.nl).

Appendix A. Supplementary material

Supplementary data associated with this article can be found, in the online version, at http://dx.doi.org/10.1016/j.jhydrol.2014.12.010.

References

Akaike, H., 1974. A new look at the statistical model identification. IEEE Trans. Autom. Control 19 (6), 716–723.
Barandiaran, D., Wang, S.-Y., Hilburn, K., 2013. Observed trends in the great pains low-level jet and associated precipitation changes in relation to recent droughts. Geophys. Res. Lett. 40, 6247–6251. http://dx.doi.org/10.1002/2013GL058296.
Berg, P., Haerter, J.O., Thejll, P., Piani, C., Hagemann, S., Christensen, J.H., 2009. Seasonal characteristics of the relationship between daily precipitation intensity and surface temperature. J. Geophys. Res. 114. http://dx.doi.org/10.1029/2009JD012008.
Browning, K.A., Pardoe, C.W., 1973. Structure of low-level jet streams ahead of mid-latitude cold fronts. Q. J. R. Meteorol. Soc. 99 (422), 619–638. http://dx.doi.org/10.1002/qj.49709942204.
Catto, J.L., Jakob, C., Berry, G., Nicholls, N., 2012. Relating global precipitation to atmospheric fronts. Geophys. Res. Lett. 39, L10805. http://dx.doi.org/10.1029/2012GL051736.
Cook, K.H., Vizy, E.K., Launer, Z.S., Patricola, C.M., 2008. Springtime intensification of the Great Plains low-level jet and Midwest precipitation in GCM simulations of the twenty-first century. J. Clim. 21, 6321–6340.
Dee, D.P. et al., 2011. The ERA-Interim reanalysis: configuration and performance of the data assimilation system. Q. J. R. Meteorol. Soc. 137 (656), 553–597.
Dettinger, M.D., Ralph, F.M., Das, T., Neiman, P.J., Cayan, D., 2011. Atmospheric rivers, floods, and the water resources of California. Water 3 (Special Issue on Managing Water Resources and Development in a Changing Climate), 455–478. http://dx.doi.org/10.3390/w3020445.
Dirmeyer, P.A., Kinter, J.L., 2009. The "Maya Express", Floods in the U.S. Midwest. Eos, Trans. Am. Geophys. Union 90 (12), 101–103.
Dobson, A.J., 2001. An Introduction to Generalized Linear Models, 2nd ed. CRC Press.
Ferrari, S.L.P., Cribari-Neto, F., 2004. Beta regression for modeling rates and proportions. J. Appl. Statist. 31 (1), 799–815.
Halverson, J.B., Rabenhorst, T.D., 2010. Mega-snow in the Megalopolis: the Mid-Atlantic's blockbuster winter of 2009–2010 Weatherwise 63, 16–23.
Hawcroft, M.K., Shaffrey, L.C., Hodges, K.I., Dacre, H.F., 2012. How much Northern Hemisphere precipitation is associated with extratropical cyclones? Geophys. Res. Lett. 39 (24). http://dx.doi.org/10.1029/2012GL053866.
Haylock, M.R. et al., 2008. European daily high-resolution gridded dataset of surface temperature and precipitation. J. Geophys. Res. 113, d20119. http://dx.doi.org/10.1029/2008JD010201.
Higgins, R.W., Shi, W., Yarosh, E., Joyce, R., 2000. Improved United States precipitation quality control system and analysis. NCEP/Climate Prediction Center Atlas 7, 40.
Klein Tank, A.M.G., Können, G.P., 2003. Trends in indices of daily temperature and precipitation extremes in Europe, 1946–99. J. Clim. 16, 3665–3680.
Lavers, D.A., Villarini, G., 2013a. Atmospheric rivers and flooding over the central united states. J. Clim. 26, 7829–7836, http://dx.doi.org/10.1175/JCLI-D-13-00212.1.
Lavers, D.A., Villarini, G., 2013b. The nexus between atmospheric rivers and extreme precipitation across Europe. Geophys. Res. Lett. 40, 3259–32644. http://dx.doi.org/10.1002/grl.50636.
Lavers, D.A., Allan, R.P., Wood, E.F., Villarini, G., Brayshaw, D.J., Wade, A.J., 2011. Winter floods in Britain are connected to atmospheric rivers. Geophys. Res. Lett. 38, L23803. http://dx.doi.org/10.1029/2011GL049783.
Lavers, D.A., Villarini, G., Allan, R.P., Wood, E.F., Wade, A.J., 2012. The detection of atmospheric rivers in atmospheric reanalyses and their links to British winter floods and the large-scale climatic circulation. J. Geophys. Res. 117, D20106. http://dx.doi.org/10.1029/2012JD018027.
McCullagh, P., Nelder, J.A., 1989. Generalized Linear Model, 2nd ed. CRC Press.
Moore, B.J., Neiman, P.J., Ralph, F.M., Barthold, F.E., 2012. Physical processes associated with heavy flooding rainfall in Nashville, Tennessee, and vicinity during 1–2 may 2010: the role of an atmospheric river and mesoscale convective systems. Mon. Weather Rev. 140 (2), 358–378.
Nakamura, J., Lall, U., Kushnir, Y., Robertson, A.W., Seager, R., 2013. Dynamical structure of extreme floods in the U.S. Midwest and the United Kingdom. J. Hydrometeorol. 14, pp. 485–288, 504.
Neiman, P.J., Ralph, F.M., Wick, G.A., Lundquist, J.D., Dettinger, M.D., 2008. Meteorological characteristics and overland precipitation impacts of atmospheric rivers affecting the West Coast of North America based on eight years of SSM/I satellite observations. J. Hydrometeorol. 9 (1), 22–47.

Neiman, P.J., Schick, L.J., Ralph, F.M., Hughes, M., Wick, G.A., 2011. Flooding in Western Washington: the connection to atmospheric rivers. J. Hydrometeorol. 12 (6), 1337–1358.

Neiman, P.J., Ralph, F.M., Moore, B.J., Hughes, M., Mahoney, K.M., Cordeira, J.M., Dettinger, M.D., 2013. The landfall and inland penetration of a flood-producing atmospheric river in Arizona. Part I: observed synoptic-scale, orographic, and hydrometeorological characteristics. J. Hydrometeor 14, 460–484, http://dx.doi.org/10.1175/JHM-D-12-0101.1.

Ospina, R., Ferrari, S.L.P., 2010. Inflated beta distributions. Stat. Pap. 23, 111–126.

Pfahl, S., Wernli, H., 2012. Quantifying the relevance of cyclones for precipitation extremes. J. Clim. 25, 6770–6780.

R Development Core Team, 2012. R: A Language and Environment for Statistical Computing. Vienna, Austria, R Foundation for Statistical Computing, URL http://www.R-project.org, ISBN 3-900051-07-0.

Ralph, F.M., Dettinger, M.D., 2012. Historical and national perspectives on extreme West Coast precipitation associated with atmospheric rivers during December 2010. Bull. Am. Meteor. Soc. 93, 783–790. http://dx.doi.org/10.1175/BAMS-D-11-00188.1.

Ralph, F.M., Neiman, P.J., Wick, G.A., Gutman, S.I., Dettinger, M.D., Cayan, D.R., White, A.B., 2006. Flooding on California's Russian River: role of atmospheric rivers. Geophys. Res. Lett. 33, L13801. http://dx.doi.org/10.1029/2006GL026689.

Rigby, R.A., Stasinopoulos, D.M., 2005. Generalized additive models for location, scale and shape. J. Roy. Stat. Soc.: Ser. C (Appl. Stat.) 54, 507–554.

Rutz, J.J., Steenburgh, W.J., 2012. Quantifying the role of atmospheric rivers in the interior western United States. Atmos. Sci. Lett. 13, 257–261.

Rutz, J.J., Steenburgh, W.J., Ralph, F.M., 2014. Climatological characteristics of atmospheric rivers and their inland penetration over the western United States. Mon. Weather Rev. 142, 905–921.

Stasinopoulos, D.M., Rigby, R.A., 2007. Generalized additive models for location scale and shape (GAMLSS) in R. J. Stat. Softw. 23 (7).

Stasinopoulos, D.M., Rigby, R.A., Akantziliotou, C, 2007. gamlss: Generalized Additive Models for Location Scale and Shape. URL <http://www.londonmet.ac.uk/gamlss/>, r package version 1.6-0.

Stasinopoulos, D.M., R. A. R. with contributions from C. Akantziliotou, G.H., Ospina, R., Motpan, N., 2009. gamlss. dist: Distributions to be used for GAMLSS modelling. URL <http://CRAN.R-project.org/package=gamlss.dist>, r package version 3.1-0.

Stewart, R.E., Szeto, K.K., Reinking, R.F., Clough, S.A., Ballard, S.P., 1998. Midlatitude cyclonic cloud systems and their features affecting large scales and climate. Rev. Geophys. 36, 245–273.

Van den Besselaar, E.J.M., Klein Tank, A.M.G., Buishand, T.A., 2013. Trends in European precipitation extremes over 1951–2010. Int. J. Climatol. 33, 2682–2689.

Viale, M., Nunez, M.N., 2011. Climatology of winter orographic precipitation over the subtropical central andes and associated synoptic and regional characteristics. J. Hydrometeorol. 12 (4), 481–507.

Yin, J.H., 2005. A consistent polewardshift of the storm tracks in simulations of 21st century climate. Geophys. Res. Lett. 32, L18701. http://dx.doi.org/10.1029/2005GL023684.

Zappa, G., Shaffrey, L.C., Hodges, K.I., Sansom, P.G., Stephenson, D.B., 2013. A multimodel assessment of future projections of North Atlantic and European extratropical cyclones in the CMIP5 climate models. J. Climate 26, 5846–5862.